Prospects for heavy neutral scalar searches at the FCC-hh

Birgit Stapf[1*], Paola Mastrapasqua[2*], Angela Taliercio[3*] and Michele Selvaggi[1*]

[1]CERN, Geneva, Switzerland.
[2]Centre for Cosmology, Particle Physics and Phenomenology (CP3), Université catholique de Louvain, Louvain-la-Neuve, Belgium.
[3]Northwestern University, Evanston, Illinois, USA.

*Corresponding author(s). E-mail(s): birgit.stapf@cern.ch; paola.mastrapasqua@cern.ch; angela.taliercio@cern.ch; michele.selvaggi@cern.ch;

1 Introduction

Searches for a heavy neutral scalar, such as an additional Higgs boson arising from singlet or doublet extensions of the Standard Model (SM), are a key aspect of Beyond the Standard Model (BSM) physics programs. These scenarios can address open questions such as the nature of electroweak symmetry breaking, the hierarchy problem, the matter-antimatter asymmetry and dark matter. The proton-proton operation phase of the Future Circular Collider (FCC-hh), with a center-of-mass energy of 84 TeV and a total dataset of 30 ab^{-1}, offers a unique opportunity to extend the mass reach of direct searches for such heavy scalars into the multi-TeV regime. Such direct searches complement high precision measurements of the Higgs sector in the search for BSM physics and thus are essential tools for mapping the Higgs potential and understanding the true nature of electroweak symmetry breaking. Here we present the expected upper limits on the cross-section (times branching ratio) for a heavy neutral scalar, H, produced in gluon-gluon fusion and coupling to either a pair of SM Higgs bosons that decays into the $b\bar{b}\gamma\gamma$ final state, or coupling to a pair of Z bosons which decay into the four lepton final state. Both of these channels benefit from a fully reconstructible final state with objects that are measured with excellent resolution, i.e. the photons and the leptons and low background contamination. Therefore they provide excellent sensitivity to heavy neutral scalar signals, despite their small branching ratio.

2 Event generation and reconstruction

The analyses reported here rely on Monte Carlo generated events for both the signal and the background processes considered. In general, all samples are generated at leading-order (LO) precision using `MadGraph5_aMC@NLO` [1] with `NNPDF2.3LO` [2]. `Pythia8` [3] is used for parton showering and hadronization effects, as well as the decays of intermediate particles to the desired final states. We assume the baseline FCC-hh operation scenario with $\sqrt{s}$= 84 TeV and an integrated luminosity of 30 ab^{-1}.

2.1 Event generation details for the $H \to hh \to b\bar{b}\gamma\gamma$ analysis

For the signal processes, only the gluon-gluon fusion induced production is considered here. The corresponding Feynman diagram, including the $H \to hh \to b\bar{b}\gamma\gamma$ decays, is shown in Figure 1a. Signal events are generated at leading order for mass points in a range of 300 GeV to 1 TeV, with increments of 50 GeV, leading to a total of 15 discrete signals. Figure 1b illustrates this by showing the reconstructed invariant mass distributions of the $b\bar{b}\gamma\gamma$ final state objects for each signal, estimating the heavy neutral scalar mass m_H . As the signals are generated under the narrow width approximation (NWA) - and any interference effects are neglected - the width of the distributions here is entirely due to assumed detector resolution.

In terms of backgrounds, only the non-resonant production of photon(s) with jets is considered here, as it is the dominant background in the mass range studied here. QCD events with two isolated, energetic photons and two jets are generated at leading order, constituting the $\gamma\gamma jj$ process, which is the main contribution to this background. To account for missing contributions from i.e. fake photons and the resonant single Higgs production mode (which contributes less than 10% of events here), as well as higher order corrections, a conservative k-factor of 2 is applied to the normalisation of the $\gamma\gamma jj$ background process.

Signals	ggH , with $m_H \in \{300,\ 350,\ 400,\ \ldots,\ 1000\}$ GeV	
Background	Cross-section [pb]	k-factor
$\gamma\gamma jj$	14.34	2.0

Table 1: Overview of signal and background samples in the $b\bar{b}\gamma\gamma$ analysis. The cross-section for the background at a center of mass energy of 84 TeV is given.

Table 1 summarizes the generated signal and background processes for the $H \to hh \to b\bar{b}\gamma\gamma$ analysis.

2.2 Event generation details for the $H \to ZZ \to 4\ell$ analysis

Again, ggF, NWA heavy scalar signals are generated at leading order. Figure 2a illustrates the process, whereas 2b shows the distributions of the reconstructed invariant four lepton mass, m_{4l}, for each discrete signal process. Here, the mass range is extended further, studying signals from 300 GeV to 10 TeV. In the low mass range, up to 1

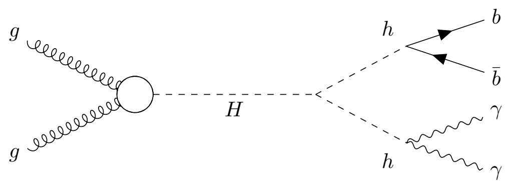

(a) Signal process

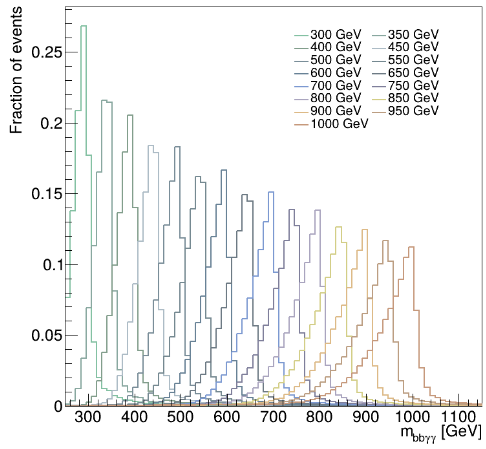

(b) Signal masses

Fig. 1: The $H \to hh \to b\bar{b}\gamma\gamma$ signals considered: 1a shows the Feynmangraph of the signal process and 1b the reconstructed invariant mass, $m_{b\bar{b}\gamma\gamma}$, distributions of all signals considered.

TeV, signals are again generated in increments of 50 GeV. Above, the step size in m_H is 0.5 TeV.

The dominant - and only - background considered in the $H \to ZZ \to 4\ell$ final state analysis is the non-resonant, continuum four lepton production. To enhance the available MC statistics in the high mass range, this process is generated in bins of the squared momentum transfer, Q^2, as indicated in Table 2. Since this process is generated at leading order, it does not include the loop-induced gluon-fusion production of a Z boson pair. A k-factor of 1.6 to correct the 4ℓ continuum normalisation to NNLO is derived from the cross-sections at 100 TeV reported in [4]. By applying it to an analysis at 84 TeV here, we assume that the relative size of the higher order corrections is independent of the center of mass energy. Further background contributions from e.g. top-quark pair or Drell-Yan production are neglected here, as they can be well-suppressed by requiring two lepton pairs compatible with an on-shell Z decay.

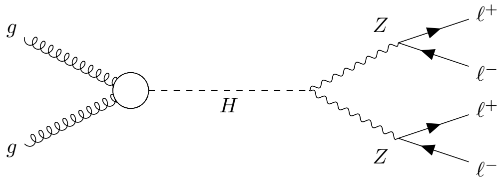

(a) Signal process

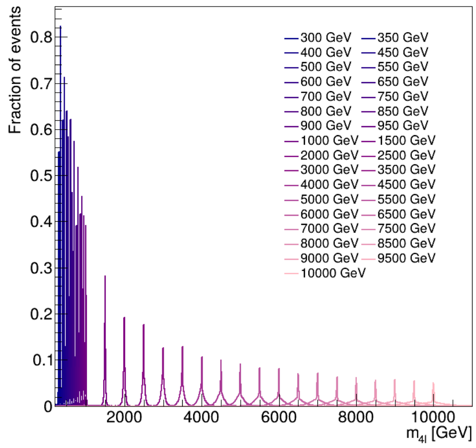

(b) Signal masses

Fig. 2: The $H \to ZZ \to 4\ell$ signals considered: 2a shows the Feynmangraph of the signal process and 2b the reconstructed invariant mass, m_{4l}, distributions of all signals considered.

2.3 Simulation and Reconstruction

A reference detector for the FCC-hh has been designed and described in the CDR [5]. All samples considered in this analysis rely on a fast simulation of this detector design with the Delphes tool [6], which describes the response of the detector components using parameterizations of the resolution and efficiency functions. Details on the specific assumptions and parameterizations for the FCC-hh reference detector scenario can be found in Ref. [7], while Ref. [6] describes the generalities of object reconstruction in Delphes.

A summary of the momentum resolutions and efficiencies of all reconstructed objects used in the two analyses presented here is given in Table 3. It should be noted that the ranges reported here cover the complete phase space in which objects are reconstructed, so also very forward or low momentum objects which are not used in the analyses. The efficiency of object isolation criteria is not included.

Signals	ggH , with $m_H \in \{300,\ 350,\ 400,\ \ldots,\ 1000\}$ GeV $m_H \in \{1.0,\ 1.5,\ 2.0,\ \ldots,\ 10\}$ TeV	
Background	$q\bar{q} \to ZZ \to 4\ell$, with	
Q^2 bin	Cross-section x BR [fb]	k-factor
0.2 - 1 TeV	751.32	1.6
1 - 3 TeV	11.197	1.6
3 - 10 TeV	0.3818	1.6
10 - 84 TeV	0.0034	1.6
Total	762.91	1.6

Table 2: Overview of signal and background samples in the $H \to ZZ \to 4\ell$ analysis. The cross-section for the background including the branching ratio to the four lepton final state at a center of mass energy of 84 TeV is given.

Object	Relative momentum resolution	Efficiency
Photons	0.2-3.0%	72-90%
Electrons	0.8-3.0%	72-90%
Muons	1.0-6.0%	88-97%%
	Medium b-tagging	76-86%
	Mistag rates c-jets	10-20%

Table 3: Ranges of the relative momentum resolutions as well as efficiencies (including reconstruction and identification efficiency) of the relevant objects as parameterized in the Delphes simulation.

Although no direct pile-up overlay is considered in the fast simulations performed here, the impact of pile-up at LHC levels is implicitly included through the Delphes parameterizations.

As reported in [8], a correction needs to be applied to the resolution of the photon angular variables in order to more accurately describe the dependence of the di-photon mass resolution on the transverse momentum. With the correction applied, the invariant mass resolution matches that obtained by the full simulation studies for the CDR [9] more closely than the pure Delphes result, i.e. the di-photon mass resolution improves with increasing transverse momentum, so here with increasing signal mass. Figure 3 shows the impact of this correction on the invariant di-photon mass distribution, $m_{\gamma\gamma}$, for an example $H \to hh \to b\bar{b}\gamma\gamma$ signal.

For the technical implementation of the event generation and simulation, the common software stack for future facilities provided by the Key4Hep framework [10, 11] is employed. In particular, the samples used here are in EDM4hep format [12]. The complete list of generated samples can be found in Ref. [13]. The samples are further processed with the FCCAnalyses framework [14], implementing the selection of final

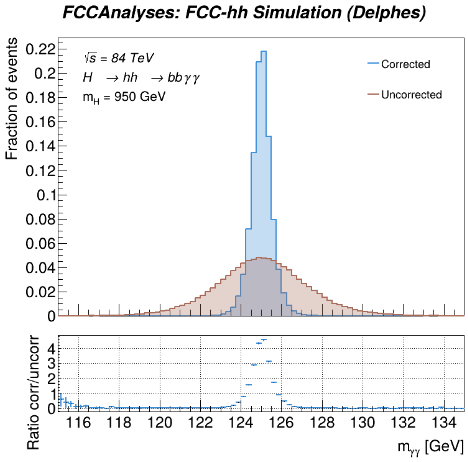

Fig. 3: Impact of the correction to the di-photon invariant mass resolution for an example $H \to hh \to b\bar{b}\gamma\gamma$ signal with a mass of 950 GeV.

state objects and events based on the criteria outlined in the respective sections 3.1 and 4.1 for the $H \to hh \to b\bar{b}\gamma\gamma$ and $H \to ZZ \to 4\ell$ analyses.

3 Analysis of the $H \to hh \to b\bar{b}\gamma\gamma$ decay channel

The $H \to hh \to b\bar{b}\gamma\gamma$ channel boosts a clean signature with well-reconstructed objects and low background rates and therefore provides excellent sensitivity despite its small branching ratio. Searches for heavy scalars decaying to a pair of Higgs boson at the LHC [15] [16] show that it provides the most stringent limits for a heavy neutral scalar that couples to a pair of Higgs boson at lower masses out of the various final states of the di-Higgs system. Here, we follow the general strategy employed for the measurement of the Higgs self-coupling in the $b\bar{b}\gamma\gamma$ final state [17]: A deep neural network (DNN) is employed to separate signal from background and the invariant mass of the di-Higgs system, $m_{b\bar{b}\gamma\gamma}$, is fitted to extract the expected upper limits on the signal cross-section.

3.1 Event selection

The final state signature of the signal is that of a pair of energetic, isolated photons, as well as a pair of b-jets, each compatible with the Higgs boson mass of 125 GeV. Table 4 gives the object and event pre-selection criteria used to target this signal signature.

The default definition and working point of the isolation for photons at the FCC-hh is employed, as given in [18], and we note that this is a point of further improvement for this analysis: the efficiency of this selection is relatively poor (averaging only around 50% for the full kinematic range of photons considered here) and we do not account for the possibility of a boosted pair of photons being reconstructed as single photon here, which means the expected sensitivity especially at high signal masses is more on

	Selection Criteria
Photons	$p_T > 30$ GeV, $\|\eta\| < 4$, Default DELPHES isolation working point
b-jets	$p_T > 30$ GeV, $\|\eta\| < 4$, Passing *medium* b-tagging requirement.
Event pre-selection	At least one pair of selected photons with $115 < m_{\gamma\gamma} < 135$ GeV, at least one pair of selected b-jets with $80 < m_{b\bar{b}} < 150$ GeV

Table 4: Object and event pre-selection criteria applied in the $H \to hh \to b\bar{b}\gamma\gamma$ analysis.

the conservative side. The same is true for the very boosted b-jets in the high mass regime, where we do not employ any of the common techniques to resolve a single-jet topology - the analysis could therefore be significantly improved with an optimization in that direction.

A simple DNN is then trained on all the signals versus the $\gamma\gamma jj$ background, using a similar set of input variables as in [17]: the number of b-jets, and angular variables of the di-photon, di-jet and di-Higgs system, such as the angular separation between the objects in each pair and the angle between the leading object and the beam axis in the rest frame of the pair. The distributions of all input variables are shown in Appendix A. Variables quantifying the transverse momenta of the respective objects and systems were not used here, as they were found to lead to sculpting effects.

Figure 4 shows the resulting DNN output score distributions for two example signals compared to that of the $\gamma\gamma jj$ background.

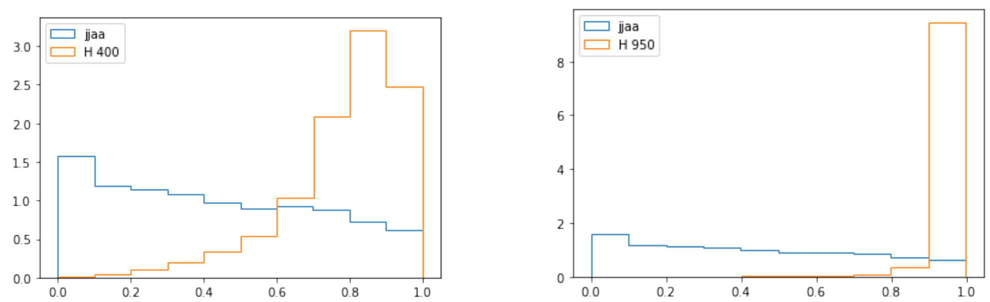

(a) m_H = 400 GeV (b) m_H = 950 GeV

Fig. 4: Distributions of the DNN output score for the $\gamma\gamma jj$ background (blue) and a signal (orange) with a mass of (a) 400 GeV and (b) 950 GeV.

Events are then selected by requiring the same minimum threshold of 0.4 on the DNN score, independent of the signal mass hypotheses. As Figure 4 exemplifies, this simple DNN approach where all signals are treated the same is not highly optimized, and leaves potential for further improvement by employing e.g. a mass dependent selection on the DNN score or a parametrized DNN to take into account the changing kinematics for different signal masses. The overall signal acceptance of the selection ranges from 6% at the lowest masses, to around 22% at the highest masses as shown in Figure 5. Here, the signal acceptance for a simple cut-based analysis imposing only a tighter selection on the di-photon and di-jet masses[1] than done on the event pre-selection is shown also for comparison. Although the cut-based approach leads to better signal acceptance at lower masses, the difference is negligible at higher masses, and the DNN approach is more performant overall due to better background suppression.

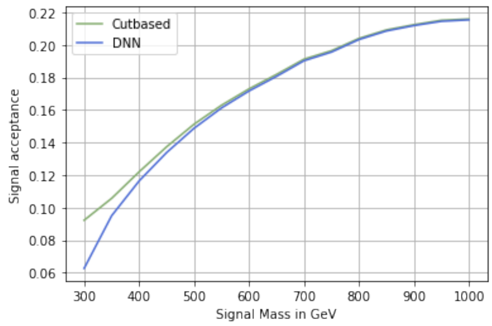

Fig. 5: Selection acceptance as a function of signal mass: the baseline analysis strategy using the DNN is compared to a simple cut-based analysis.

3.2 Fitting strategy and systematic uncertainties

For each signal mass hypothesis, the 95% CL limit is derived by fitting the distributions of the invariant mass of the $b\bar{b}\gamma\gamma$ system, $m_{b\bar{b}\gamma\gamma}$. The respective fitting range is defined as $m_H \pm 0.3 \times m_H$. Figure 6 shows the resulting distributions for two example signal masses.

Systematic uncertainties accounting for reconstruction and measurement effects are assumed on the signal and background. We study only one benchmark scenario of systematic uncertainties, which corresponds to "Syst. 2" in the $b\bar{b}\gamma\gamma$ self-coupling analysis [17]. A 1% uncertainty is assumed on the overall luminosity measurement, as well as the reconstruction and identification efficieny of each photon and b-jet. These uncertainties are applied to signal only. In contrast, we assume that the background will be constrained from the sidebands in the $m_{b\bar{b}\gamma\gamma}$ fit leading to a data-driven estimate - to account for this effect, its normalization is left free to float within 5%. Table 5 summarizes the systematic uncertainties. No theory uncertainties on the signal normalisation are assumed.

[1]The specific cut-based selection is: $122 < m_{\gamma\gamma} < 128$ GeV and $90 < m_{\gamma\gamma} < 130$ GeV

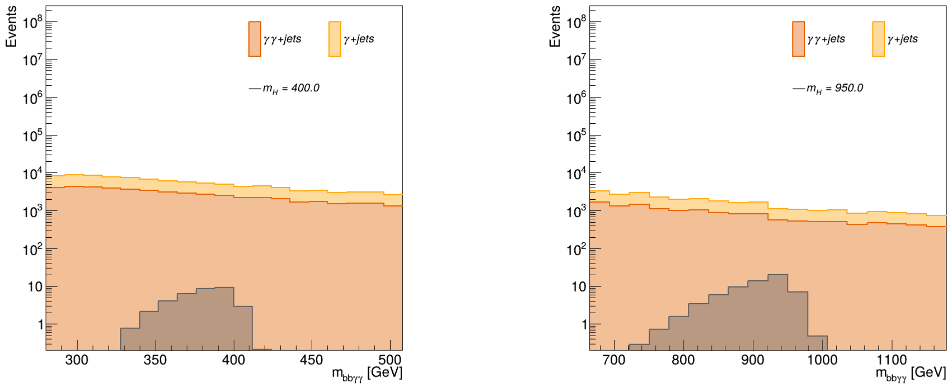

(a) m_H = 400 GeV

(b) m_H = 950 GeV

Fig. 6: Distributions of the invariant mass of the di-Higgs system, $m_{b\bar{b}\gamma\gamma}$, in the fitting range for the background and a signal with a mass of (a) 400 GeV and (b) 950 GeV. Signal events are normalised to a cross-section of 1 ab.

Source of uncertainty	Value	Type	Applies to
b-jet ID / b-jet	1%	lnN	Signal
Photon ID / lepton	1%	lnN	Signal
Luminosity	1%	lnN	Signal
Data-driven bkg. est.	5%	lnU	Non-resonant bkg, $\gamma\gamma jj$

Table 5: Overview of systematic uncertainties considered.

3.3 Results

The resulting upper limit on the signal cross-section times branching ratio into a Higgs boson pair, $\sigma(pp \to H \to hh)$, as a function of the signal mass is shown in Figure 7. It ranges from 90 fb at 300 GeV, to 10 fb at 1 TeV. The sensitivity increases with increasing mass, due to the steeply dropping off background but also due to the increased signal acceptance for higher masses.

4 Analysis of the $H \to ZZ \to 4\ell$ decay channel

Similarly to the $b\bar{b}\gamma\gamma$ final state, the $H \to ZZ \to 4\ell$ channel is rare but profits from low backgrounds and the fully reconstructible final state of four well measured leptons. The large data statistics of the FCC-hh program are ideal to exploit this in order to achieve stringent upper limits. Here we employ a simple cut-based analysis, and fit the four-lepton invariant mass, m_{4l}, to obtain the upper limits.

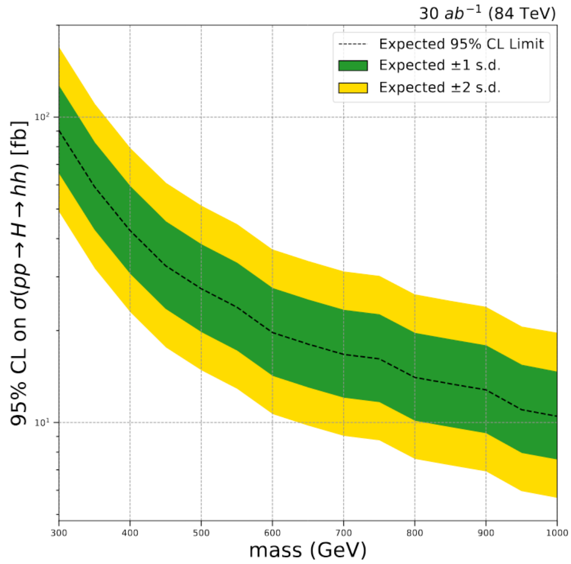

Fig. 7: Upper limit following the 95% CL procedure on the signal cross-section times branching ratio into a Higgs boson pair as a function of signal mass.

4.1 Event selection

The first step of the event selection on the $H \to ZZ \to 4\ell$ analysis is building the two opposite sign, same flavour (OSSF) lepton pairs that make up the signal final state. Here, we follow the same approach to identify these pairs as in the SM Higgs projections for FCC-hh [19]: Isolated muons and electrons (again using the default working point) within a pseudo-rapidity of 4 are selected as the basis to build the two pairs. Muons take precedence in the pair building - if there are two OS muon pairs fulfilling the requirements those two will be selected, and only if there aren't electron pairs will be selected. No further ambiguity resolution is employed. The pair with the higher lepton transverse momenta is referred to as the leading pair, with leptons ℓ_1 and ℓ_2, while the subleading pair consists of leptons ℓ_3 and ℓ_4. Table 6 shows the transverse momentum requirements the selected lepton pairs need to pass. The resulting distributions of the flavour composition of the pair - 4μ, $2e2\mu$ or $4e$ - is shown in Figure 8a. Due to the higher muon efficiencies and their priority in the pair building strategy, 4μ events are more common than $4e$ events.

For the cut-based event selection we require that both lepton pairs are compatible with an on-shell Z decay in a relatively narrow window. LHC searches for heavy scalars in the $H \to ZZ \to 4\ell$ channel typically employ more complex event selection strategies, i.e. the studies reported in [20] rely on multivariate classifiers which exploit the signal event kinematics such as various angular variables of the four-lepton system, and allow to categorize events into different production modes. We only study the

	Selection Criteria
Leptons pre-selection	$p_T > 5$ GeV, $\|\eta\| < 4$, Default DELPHES isolation working point
Leading lepton pair	$p_T(\ell_1) > 20$ GeV, $p_T(\ell_2) > 15$ GeV,
Subleading lepton pair	$p_T(\ell_3) > 10$ GeV, $p_T(\ell_4) > 5$ GeV.
Event selection	At least two OSSF lepton pairs, with $80 < m_{ll} < 100$ GeV in both pairs, $\|\cos(\theta^*)\| < 0.8$

Table 6: Object and event selection criteria applied in the $H \to ZZ \to 4\ell$ analysis.

sensitivity to the ggF signal mode here, and apply only one additional event selection criterion based on the the production angle of the leading Z defined the four-lepton rest frame, $\cos(\theta^*)$, as reported in Table 6. The corresponding distributions of all event selection variables for an example signal are shown in Figure 8b- 8d. The selection on $\cos(\theta^*)$is able to nearly half the 4ℓ continuum background, while retaining around 80% of the signal across the whole mass range.

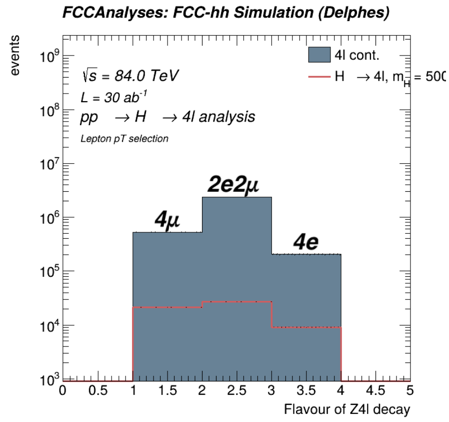

(a) Flavour composition

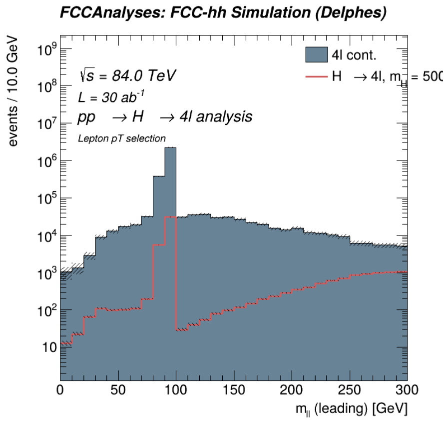

(b) m_{ll} leading pair

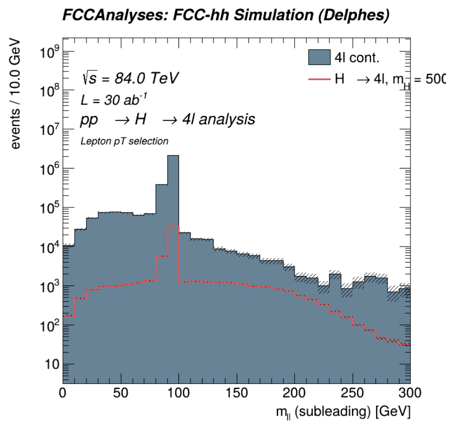

(c) m_{ll} subleading pair

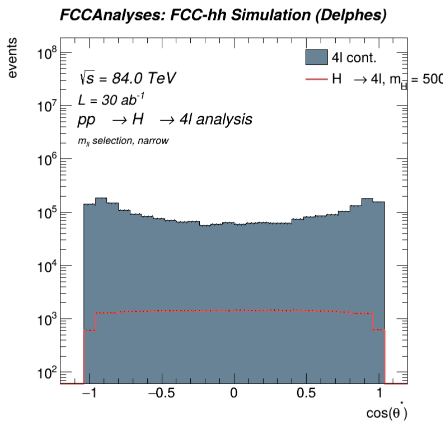

(d) $\cos(\theta^*)$

Fig. 8: Distributions in the analysis for an example signal with a mass of 500 GeV: (a) The lepton flavour composition of the selected pairs, and the event selection variables, with the previous selection applied (b) the invariant mass of the leading lepton pair, (c) the invariant mass of the subleading lepton pair and (d) the production angle of the leading Z defined the four-lepton rest frame, $\cos(\theta^*)$. The signal is normalised to a cross-section of 1 ab.

Nonetheless, the event selection is not optimal and leaves room for improvement by e.g. employing machine learning techniques here as well. Figure 9 shows the signal acceptance as a function of mass - as can be seen, overall the signal acceptance is fairly low ranging from 8.5% to 10.5% only. Moreover it shows a decline with increasing mass beyond 5 TeV, which would likely be able to be recovered by more dedicated analyses techniques for the case of lepton pairs that are so boosted they are reconstructed as a single object.

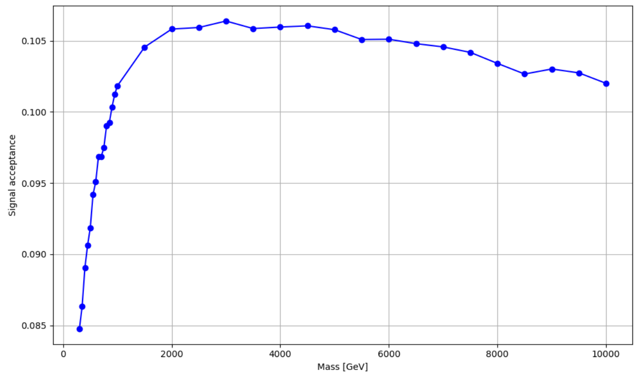

Fig. 9: Selection acceptance as a function of signal mass in the cut-based $H \to ZZ \to 4\ell$ analysis.

4.2 Fitting strategy and systematic uncertainties

For each signal mass hypothesis, the 95% CL limit is derived by fitting the distributions of the invariant mass of the four lepton system, m_{4l}. The respective fitting range is defined as $m_H \pm 0.3 \times m_H$. Figure 10 shows the resulting distributions for two example signal masses.

The systematic uncertainties in the $H \to ZZ \to 4\ell$ analysis follow the same assumptions as already described for the $H \to hh \to b\bar{b}\gamma\gamma$ analysis in Section 3.2 : A 1% uncertainty is assumed on the overall luminosity measurement, as well as the reconstruction and identification efficiency of each lepton. These uncertainties are applied to signal only. In contrast, we assume that the background will be constrained from the sidebands in the m_{4l} fit leading to a data-driven estimate - to account for this effect, its normalization is left free to float within 5%. Table 7 summarizes the systematic uncertainties. No theory uncertainties on the signal normalisation are assumed.

Source of uncertainty	Value	Type	Applies to
Lepton ID / lepton	1%	lnN	Signal
Luminosity	1%	lnN	Signal
Data-driven bkg. est.	5%	lnU	4ℓ continuum bkg.

Table 7: Overview of systematic uncertainties considered.

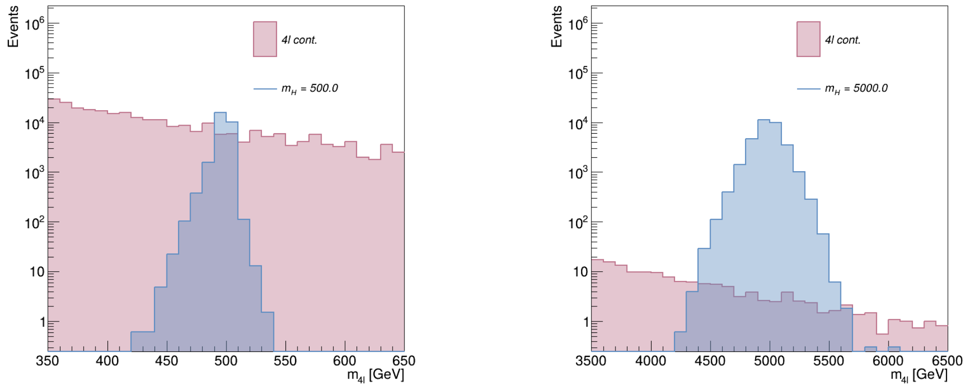

(a) $m_H \ = 500$ GeV (b) $m_H \ = 5$ TeV

Fig. 10: Distributions of the invariant mass of the four lepton system, m_{4l}, in the fitting range for the background and a signal with a mass of (a) 500 GeV and (b) 5 TeV. Signal events are normalised to a cross-section of 1 ab.

4.3 Results

The resulting upper limit on the signal cross-section times branching ratio into a Higgs boson pair, $\sigma(pp \to H \to ZZ)$, as a function of the signal mass is shown in Figure 11. It ranges from 20 fb at 300 GeV, to 0.1 fb at 10 TeV - the $H \to ZZ \to 4\ell$ channel is therefore more sensitive than the $H \to hh \to b\bar{b}\gamma\gamma$ channel.

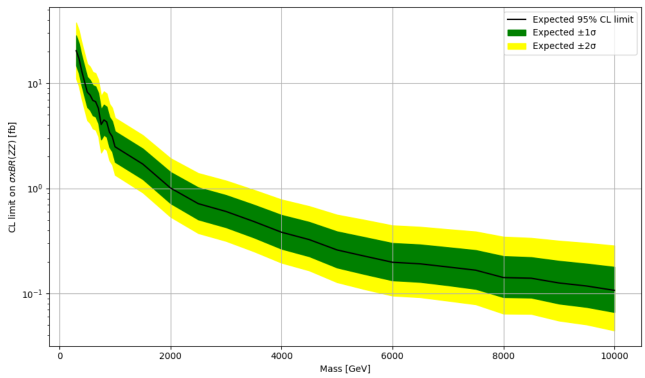

Fig. 11: Upper limit following the 95% CL procedure on the signal cross-section times branching ratio into a Z boson pair as a function of signal mass.

5 Conclusion

In this note, we have presented the prospects for a search for a heavy neutral scalar boson produced via gluon-gluon fusion, decaying either into a pair of Higgs bosons or into a pair of Z bosons in the $H \to hh \to b\bar{b}\gamma\gamma$ and $H \to ZZ \to 4\ell$ final state respectively. The study is based on simulated proton-proton collision data at a center-of-mass energy of $\sqrt{s} = 84$ TeV, representative of the expected baseline operation of the FCC-hh.

Upper limits at 95% confidence level are set on the production cross-section times branching ratio, $\sigma(pp \to H \to hh)$ and $\sigma(pp \to H \to ZZ)$, as a function of the heavy scalar mass. In the $H \to hh \to b\bar{b}\gamma\gamma$ channel, cross-section upper limits range from 90 to 10 fb for masses between 300 GeV and 1 TeV. In the $H \to ZZ \to 4\ell$ channel, limits range from 20 to 0.1 fb over the mass range 300 GeV to 10 TeV.

The analyses were not highly optimized, and the upper limits should therefore be understood to be on the conservative side, serving as a first estimate of the FCC-hh mass reach in these specific channels. There is significant potential for improvement of the analysis techniques, especially to address the relatively inefficient reconstruction of photons and leptons, and employing dedicated methods to treat boosted, overlapping decay products at high signal masses.

Nevertheless, these results demonstrate the sensitivity of the FCC-hh to rare multi-boson final states and the excellent prospects for direct searches up to masses of several TeV it provides.

Acknowledgements

This work has been partly supported by the Future Circular Collider Innovation Study (FCCIS) project, that has received funding from the European Union's Horizon 2020 research and innovation programme under grant No 951754.

A $H \to hh \to b\bar{b}\gamma\gamma$ DNN input features

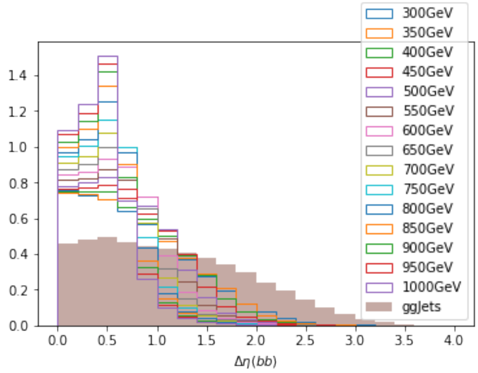

(a) $\Delta\eta$ between the jet candidates.

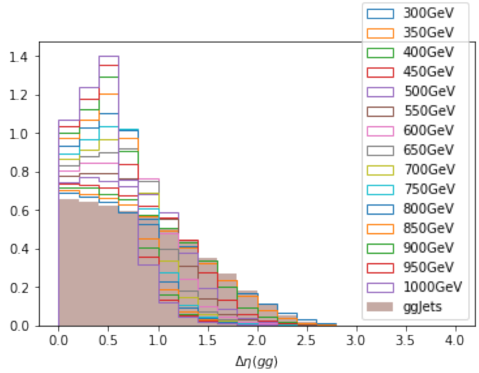

(b) $\Delta\eta$ between the photon candidates.

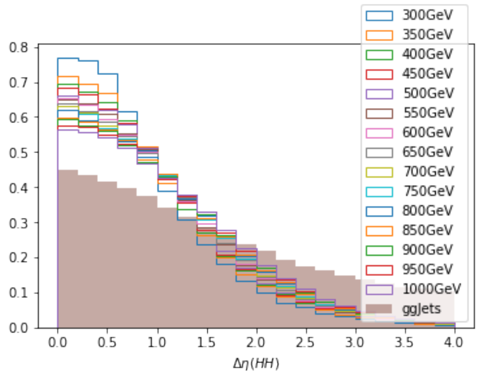

(c) $\Delta\eta$ between the Higgs candidates.

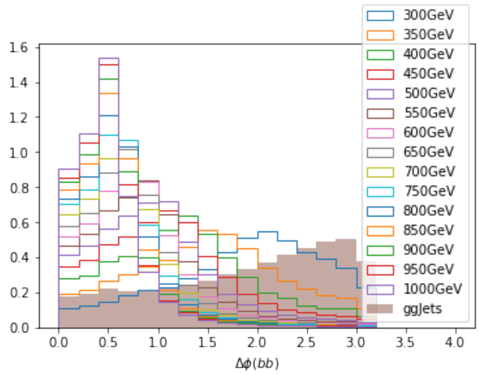

(d) $\Delta\phi$ between the jet candidates.

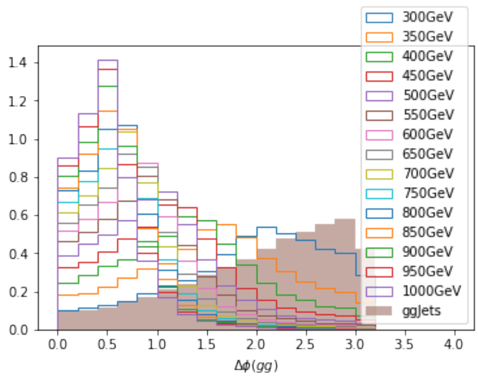

(e) $\Delta\phi$ between the photon candidates.

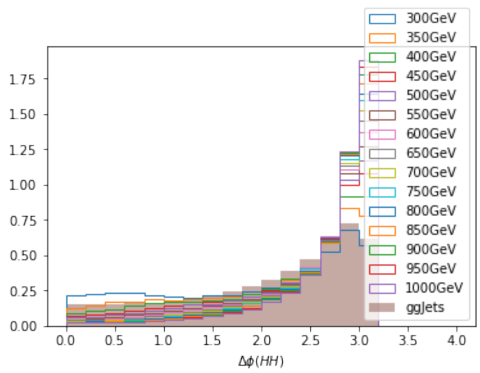

(f) $\Delta\phi$ between the Higgs candidates.

Fig. 12: DNN input features in the $b\bar{b}\gamma\gamma$ analysis (1/2).

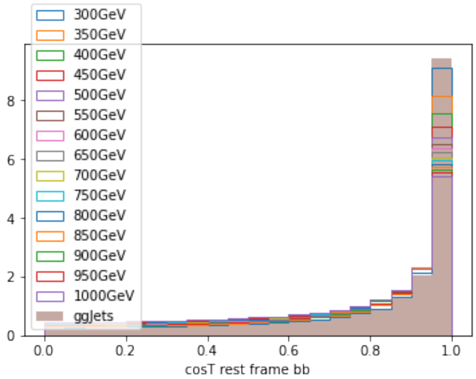

(a) Angle between the leading jet and the beam axis in the di-jet rest frame.

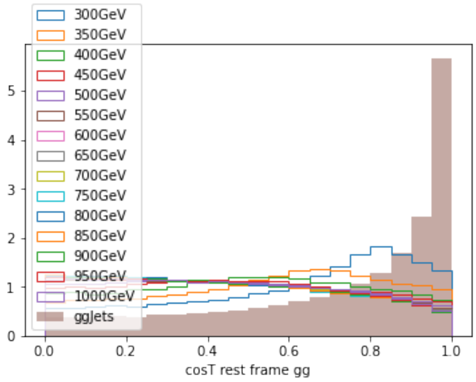

(b) Angle between the leading photon and the beam axis in the di-photon rest frame.

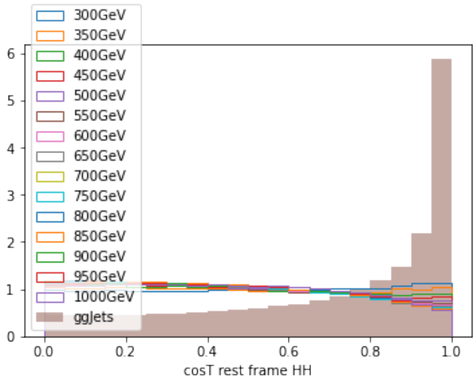

(c) Angle between the di-photon and the beam axis in the di-Higgs rest frame.

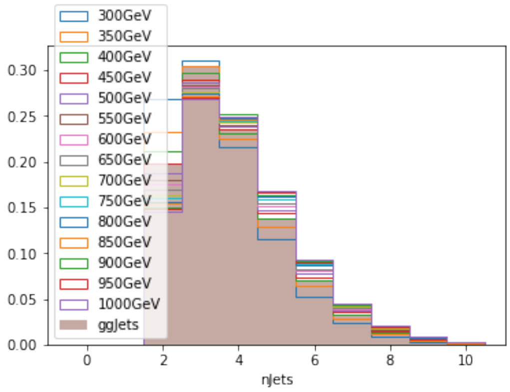

(d) Number of b-tagged jets.

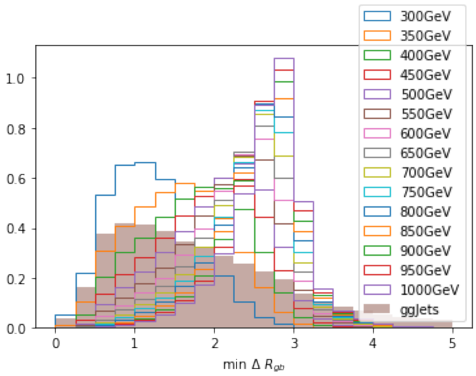

(e) ΔR between the closest photon-jet pair.

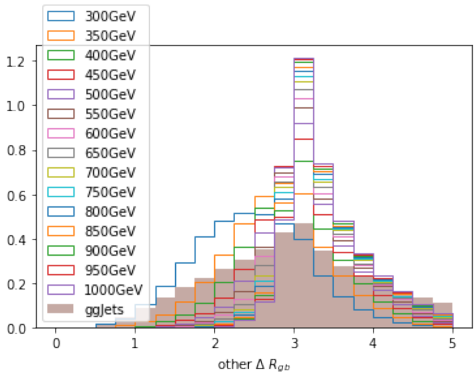

(f) ΔR between the other photon-jet pair.

Fig. 13: DNN input features in the $b\bar{b}\gamma\gamma$ analysis (2/2).

References

[1] J. Alwall, et al., The automated computation of tree-level and next-to-leading order differential cross sections, and their matching to parton shower simulations. JHEP **07**, 079 (2014). https://doi.org/10.1007/JHEP07(2014)079. arXiv:1405.0301 [hep-ph]

[2] R.D. Ball, V. Bertone, S. Carrazza, L. Del Debbio, S. Forte, A. Guffanti, N.P. Hartland, J. Rojo, Parton distributions with qed corrections. Nuclear Physics B **877**(2), 290–320 (2013). https://doi.org/10.1016/j.nuclphysb.2013.10.010. URL http://dx.doi.org/10.1016/j.nuclphysb.2013.10.010

[3] C. Bierlich, et al., A comprehensive guide to the physics and usage of PYTHIA 8.3. SciPost Phys. Codeb. **2022**, 8 (2022). https://doi.org/10.21468/SciPostPhysCodeb.8. arXiv:2203.11601 [hep-ph]

[4] M. Mangano. Physics at the FCC-hh, a 100 TeV *pp* collider (2017). URL https://cds.cern.ch/record/2270978

[5] A. Abada, et al., FCC-hh: The Hadron Collider: Future Circular Collider Conceptual Design Report Volume 3. Eur. Phys. J. ST **228**, 755 (2019). https://doi.org/10.1140/epjst/e2019-900087-0

[6] J. de Favereau, et al., DELPHES 3, A modular framework for fast simulation of a generic collider experiment. JHEP **02**, 057 (2014). arXiv:1307.6346 [hep-ex]

[7] M. Selvaggi, B. Stapf. A Delphes parameterisation of the FCC-hh detector (2025). https://doi.org/10.17181/71pv5-tvf87

[8] E. Mazzeo, S. Manzoni, B. Stapf. Measurement of the $t\bar{t}H$ production in diphoton final states at the FCC-hh (2025). https://doi.org/10.17181/tr6k7-bm770

[9] M. L. Mangano, et al., Conceptual design of an experiment at the FCC-hh, a future 100 TeV hadron collider. Tech. rep. (2022). https://doi.org/10.23731/CYRM-2022-002. URL https://cds.cern.ch/record/2842569

[10] P. Fernandez Declara, et al., The Key4hep turnkey software stack for future colliders. PoS **EPS-HEP2021**, 844 (2022). https://doi.org/10.22323/1.398.0844

[11] B. Francois, G. Ganis. The FCC software for PED studies (2024). https://doi.org/10.17181/8k0c4-nkr70

[12] *EDM4hep data model*. https://edm4hep.web.cern.ch/

[13] B. Stapf, J. Smiesko. List of fcc_v07 official FCC-hh production samples (2025). https://fcc-physics-events.web.cern.ch/fcc-hh/delphes/fcc-v07/ii or https://fcc-physics-events.web.cern.ch/fcc-hh/Delphesevents_fcc_v07/II.php

[14] C. Helsens, E. Perez, M. Selvaggi, V. Volkl, L. Forthomme, J. Munch Torndal. HEP-FCC/FCCAnalyses: v0.10.0 (2024). URL https://doi.org/10.5281/zenodo.13871482

[15] ATLAS collaboration, Combination of Searches for Resonant Higgs Boson Pair Production Using pp Collisions at $\sqrt{s}$ =13 TeV with the ATLAS Detector. Phys. Rev. Lett. **132**(23), 231801 (2024). https://doi.org/10.1103/PhysRevLett.132.231801. arXiv:2311.15956 [hep-ex]

[16] The CMS collaboration, Searches for Higgs boson production through decays of heavy resonances. Phys. Rept. **1115**, 368–447 (2025). https://doi.org/10.1016/j.physrep.2024.09.004. arXiv:2403.16926 [hep-ex]

[17] A. Taliercio, P. Mastrapasqua, B. Stapf, M. Selvaggi. Higgs self-coupling determination in the $bb\gamma\gamma$ final state at the FCC-hh (2025). https://doi.org/10.17181/w6928-gr929

[18] Delphes card for FCC-hh scenario II. https://github.com/delphes/delphes/blob/master/cards/FCC/scenarios/FCChh_II.tcl

[19] B. Stapf, M. Selvaggi, J. Eysermans. Measurements of rare higgs decay couplings at the fcc-hh (2024). https://doi.org/10.17181/sxreb-8h751

[20] ATLAS collaboration, Search for heavy resonances decaying into a pair of Z bosons in the $\ell^+\ell^-\ell'^+\ell'^-$ and $\ell^+\ell^-\nu\bar{\nu}$ final states using 139 fb^{-1} of proton–proton collisions at $\sqrt{s}$ = 13 TeV with the ATLAS detector. Eur. Phys. J. C **81**(4), 332 (2021). https://doi.org/10.1140/epjc/s10052-021-09013-y. arXiv:2009.14791 [hep-ex]